

Integration of a Thermal Imaging Feedback Control System in Electron Beam Melting

Emmanuel Rodriguez¹, Francisco Medina¹, David Espalin¹, Cesar Terrazas¹, Dan Muse¹, Chad Henry², Eric MacDonald¹, and Ryan B. Wicker¹

¹W.M. Keck Center for 3D Innovation, The University of Texas at El Paso, El Paso, TX 79968, USA

²Lockheed Martin Aeronautics Company, Marietta, GA 30063, USA

REVIEWED, Accepted August 15, 2012

Abstract

A thermal imaging system using an infrared (IR) camera was incorporated in the fabrication process of an Arcam A2 Electron Beam Melting system to provide layer-by-layer feedback and ensure quality and defect free products. Using the IR camera, build chamber surface temperature profiles were imaged and analyzed, providing information used to modify build settings for the next build layer. Individual part temperatures were also monitored and modified to achieve a more uniform bed temperature. The thermal imaging information can also be used as a quality control tool to detect imperfections during the build. Results from the integration of the camera in the system as well as use of the thermal images in process monitoring and control is described.

Introduction

The Electron Beam Melting (EBM) process is a promising technology in the rapid manufacturing of metal components. EBM has the potential to reduce the cost of metal parts by minimizing the use of raw materials and machining time. The EBM technology has several advantages over other additive manufacturing (AM) technologies of metal, such as manufacturing speed and mechanical properties of the finished parts. For the process to be accepted in the aerospace industry as a flight-ready manufacturing technology, however, improved control and feedback must be implemented in the building process for better part quality and manufacturing repeatability. As part of this research, an IR imaging system was implemented in an *Arcam A2 EBM* system providing another level of control for the EBM process that could lead to rapid certification of flight-ready parts.

The EBM technology is a relatively new direct-metal freeform fabrication process that has been commercialized by *Arcam* [1]. The machine uses a metal powder (10 μm - 160 μm diameter) to build solid parts in layer-wise fashion inside a vacuum chamber maintained at $\leq 1.5 \times 10^{-3} \text{mbar}$ (Figure 1) by following 4 steps: 1) spreading a layer of metal powder (typically in the range 0.05 – 0.20 mm thick) across the build platform by using the machine's raking mechanism, 2) preheating the layer to approximately 50% of the metal's melting temperature (760°C for Ti6Al4V) using the electron beam gun at relatively low beam current and high scan speed (the preheating step lightly sinters the metal powder to hold it in place for subsequent melting and also transmits heat to the part that helps maintain a low thermal gradient

between the melted layer and the rest of the part- greatly reducing residual stresses), 3) selectively melting the preheated powder by increasing the beam power and reducing the scan speed to effectively reach the material's melting point, and 4) lowering the build platform an amount equal to one layer thickness [1]. The process is repeated until the part is complete.

In thermodynamics, temperature is an important state variable that can be used to help determine energy states as well as assist in determination of heat transfer, and as a result, the measurement, monitoring, and control of temperature is an important variable in the evolution of the metal during EBM fabrication. The distribution of temperatures on the powder bed surface of the EBM platform should be as uniform as possible to achieve equal part quality, characteristics, and properties [1]. However, the lack of spatial feedback of temperature from the A2 system (since a single thermocouple located below the build plate is used to monitor temperature) leads to the notion of non-uniform temperature distribution within the build chamber. As a result, a reliable temperature monitoring system is desired to more effectively control build temperatures during fabrication. Infrared (IR) thermal imaging has been chosen as the most suitable feedback system for this application due to the ability of measuring two-dimensional surface temperatures and inspection capabilities of part defects. Moreover, correlations between process build parameters and the temperature of the melt pool can be determined with thermal imaging [2].

The focus of the current project is to obtain true temperatures from the IR images acquired. Using the measured temperatures, real-time individual part parameter modification was implemented to achieve a more uniform temperature surface for all parts in the build. Real temperature measurements may also be used, although not the focus of the current project, to make a correlation between a part's mechanical properties and microstructure. Recent work has been successful in identifying part defects with the use of thermal imagery [3], a brief investigation on the methodology of quantifying these defects and correcting them in successive layers in real-time is also discussed.

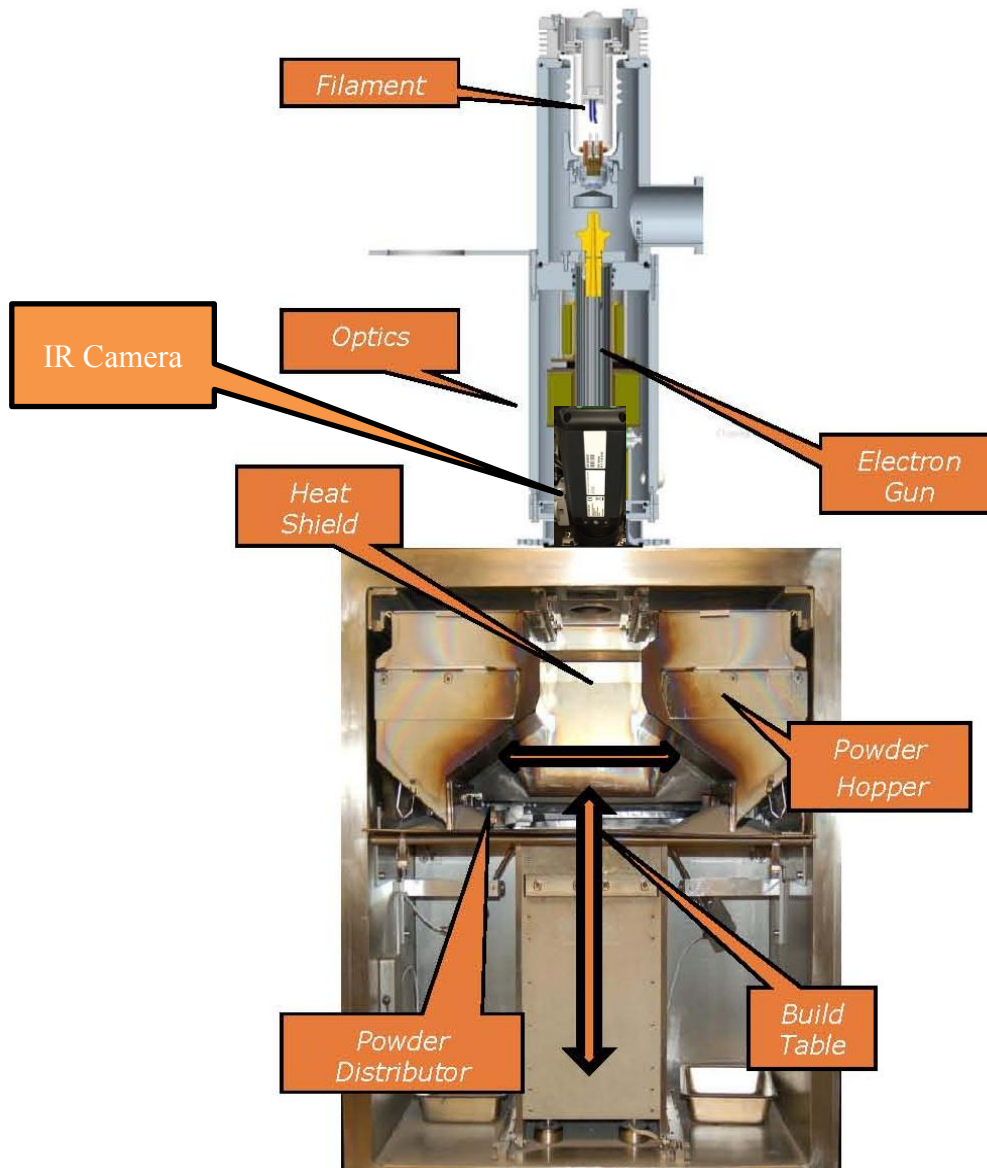


Figure 1 Arcam A2- build chamber

Thermal-Imaging System Integration into Arcam A2

A FLIR SC645 (FLIR Systems AB, Sweden) IR camera was selected for integration in the Arcam A2 system based on its measurement temperature range (up to 2000 °C [5]), high resolution (640 x 480), and the necessary field of view with the default 25° lens. The location of the camera to the powder bed is approximately 330 mm, resulting in a field of view of 274 mm x 206 mm, and a spatial resolution of 350 um/pixel. Several machine modifications were required to successfully integrate the FLIR SC645 IR camera for monitoring the surface of the build

chamber. First, there were a number of items removed to make way for the drilling of new holes for the flap mechanism and actuator. The upper and lower chamber door cowling, column turbo pump, and column assembly with film drive were all removed. Five precise (± 0.02 mm) holes were drilled atop the build chamber. It is important to note that these holes were drilled with circumspection to preserve the high vacuum requirements ($\leq 1.5 \times 10^{-3} \text{ mbar}$) within the electron beam melting build chamber. The components were then reinstalled, and an additional chamber frame that is used to hold the FLIR camera mount was also put in place.

Several components were required to be incorporated into the modified system to make the acquisition of IR images of the system's build surface possible (Figure 2). A zinc-selenide (ZnSe) glass with O-rings above and below the glass replaced the system's film camera. The ZnSe glass is the viewing window of the camera allowing transmittance in the IR spectrum. The transmittance was calculated to be 94% by measuring the temperature of a hot plate in the chamber - with and without the window for comparison. The ZnSe window needs to be protected from metallization during the melting process, and to do this, a protective flap that acts as a shutter was installed inside the chamber. The flap is held in place with a feed-thru mechanism, sealed with an O-ring, and a feed-thru collar holds this in place. A pneumatic piston is used to open and close the shutter (flap) to permit image capture when the beam is off. Air supply is connected to the input regulator on the pneumatic panel. The pneumatic panel is powered by tapping into the chamber vacuum gauge in the wire breakout panel on the wall of the chamber cabinet. A parallel cable is run from the D-sub connector in the electronics rack to the connection box on the pneumatic panel and the pneumatic piston is connected to the pneumatic panel. Once powered, the flap is in the closed position and the micro-switch is in the 'normally closed' state allowing the beam to become active. The IR camera is now put in position for image capture as shown in Figures 1 and 2. The angle between the camera and the surface normal is 25° , which according to the IR camera's manufacturer, an angle below 30° will neglect the effect of temperature deviation between the measured temperature and the real temperature value [5].

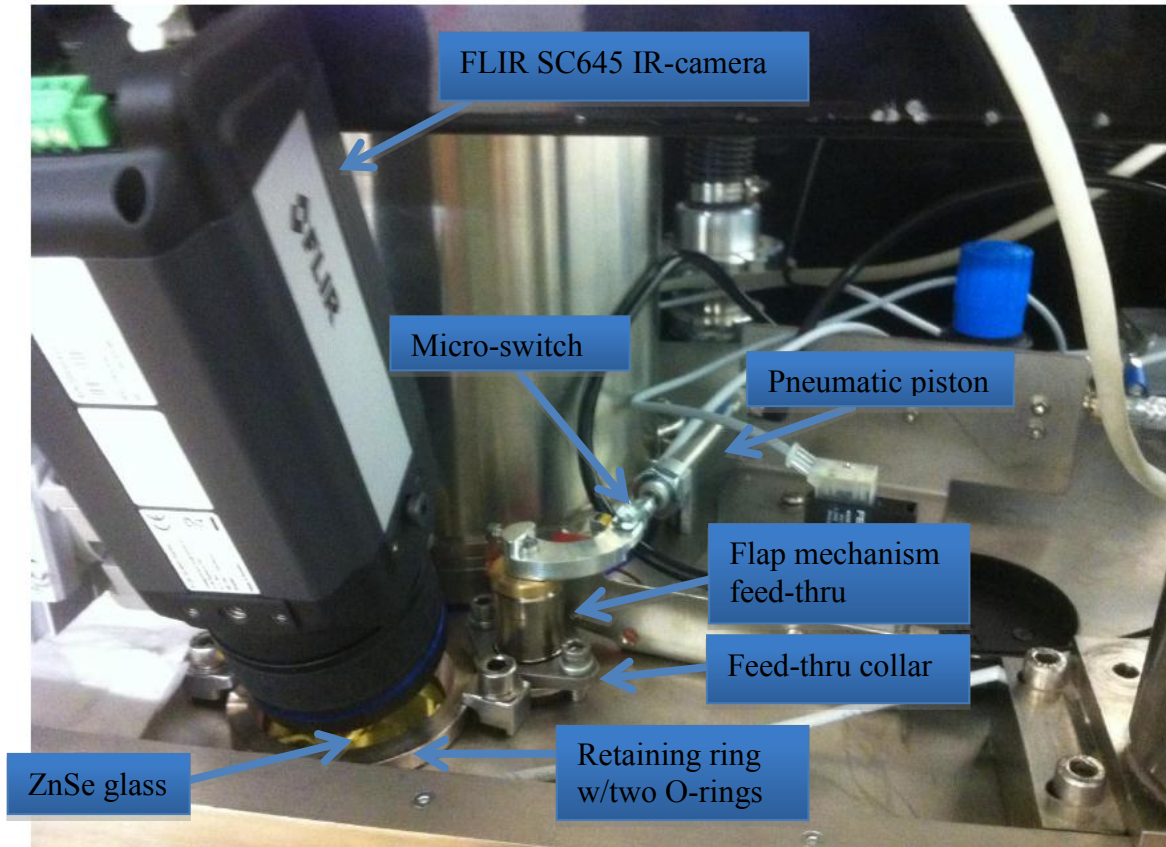


Figure 2 Top of Arcam-A2's build chamber with new component location and IR-camera

In order to automate the opening of the flap mechanism (or shutter), monitoring of a voltage signal from the *Arcam* system was required. This signal was received and interpreted by a modular controller from National Instruments (NI cRIO-9074, Austin, TX). These signals were then incorporated into the standard process steps (first is a preheat step, followed by the melt step) for a given layer. There are three different process signals that can be used during the build process for a layer. For example, signal one can be assigned to assert before the preheat step, signal two before the melt, and signal three after the melt. A collaborative effort with *Arcam AB* resulted in a new version of the *EBM Control software* that allows the selection of these process steps to be incorporated into the standard process step cycle. Figure 3 is a schematic of the architecture for the IR feedback control in the *A2* system.

To complete the implementation of a feedback control system, the next step was to intercept the output signals from the *A2*'s output module. The intercepted signal is fed to an electromechanical relay (opens/closes the flap mechanism) that connects to the modular controller. The NI cRIO-9074 controller is the central unit for feedback from the *A2* system. This unit allowed the attachment of various modules to realize tasks such as measuring signals and issuing commands. Once the controller received the signal to open the shutter, *LabVIEW*

was used to program the IR camera to render a snapshot of the surface bed. Thermal images are recorded, archived, processed and analyzed.

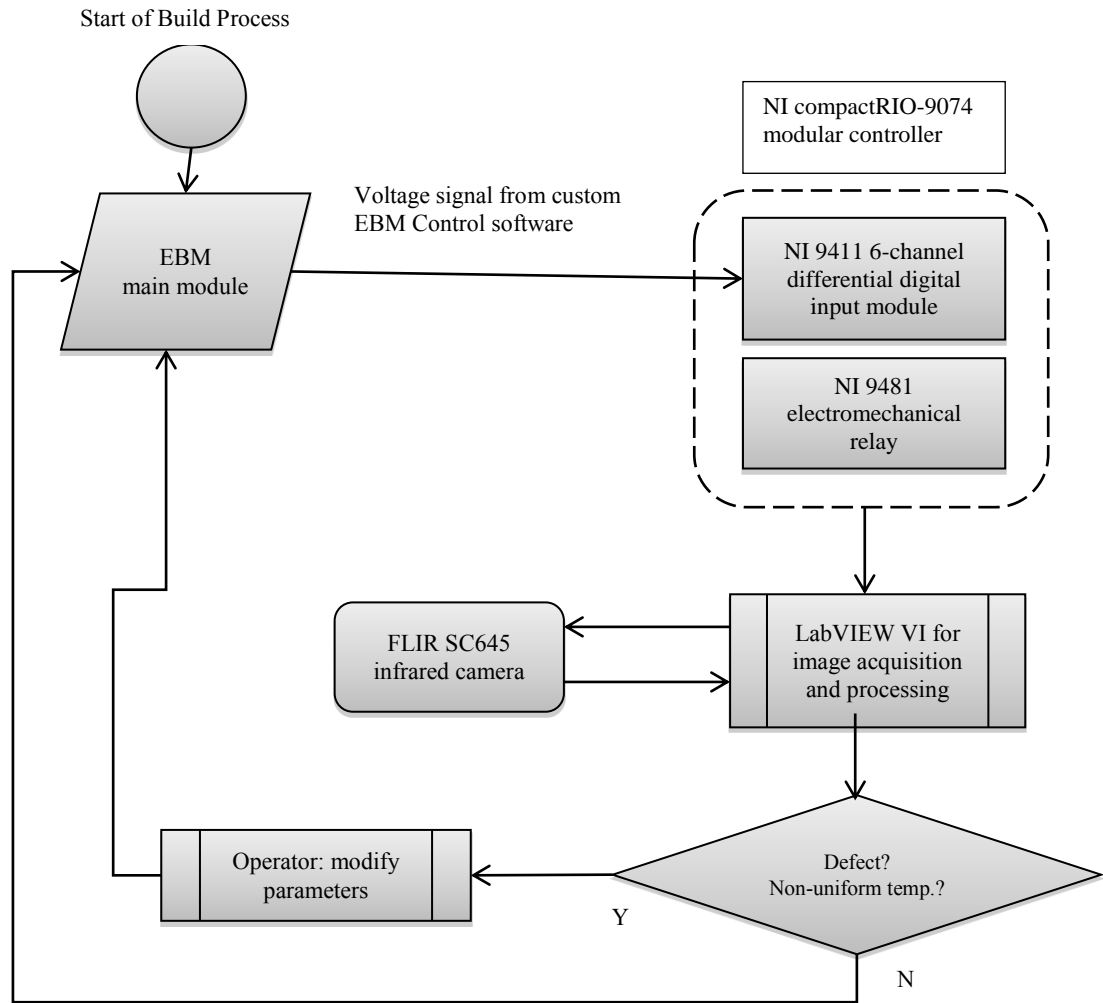


Figure 3 Architecture for IR feedback control in Arcam A2 system

IR Camera Calibration

The FLIR SC645 used here images and measures the emitted IR radiation from an object. As shown in Figure 4, the radiation measured by the camera is made up of emission from the object $\epsilon\tau W_{obj}$, reflected emission from ambient sources $(1 - \epsilon)\tau W_{refl}$, and emission from the atmosphere $(1 - \tau)W_{atm}$. For the camera to measure temperature accurately, the following parameters are required to be known and supplied to the camera: emissivity of the object, reflected apparent temperature, and temperature of the atmosphere.

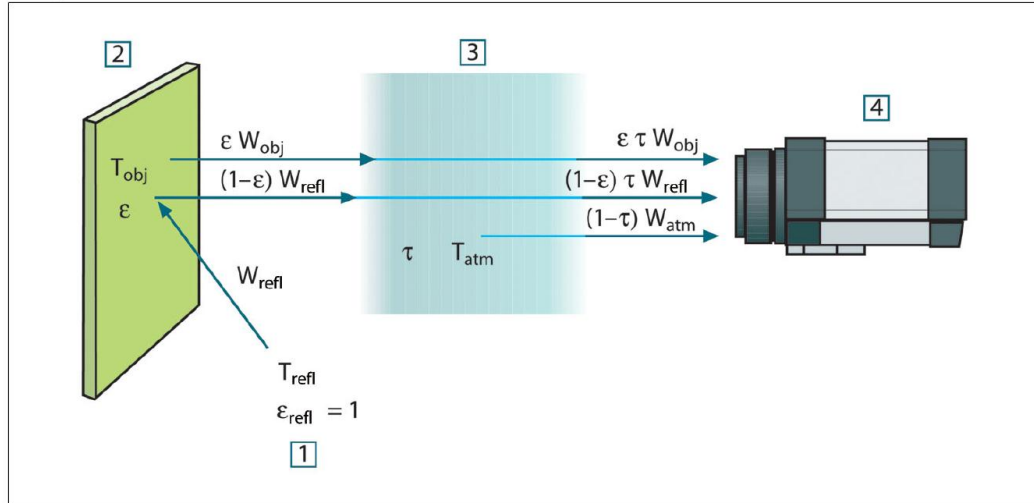


Figure 4 A schematic representation of the general thermographic measurement situation. 1: Surroundings, 2: Object, 3: Atmosphere, 4: Camera. Courtesy: FLIR Systems AB

Figure 4 shows three different sources of power W that the IR camera receives and translates to a camera signal U that is proportional to the power input (power linear camera) [5]. The signal U is obtained by multiplying a constant C (FLIR Systems AB) by the radiation power W [4]. The total received radiation power can now be written in terms of the total measured camera output voltage U_{tot} .

$$U_{tot} = \varepsilon\tau U_{obj} + (1 - \varepsilon)\tau U_{refl} + (1 - \tau)U_{atm}$$

Here, ε is the emissivity of the object and τ is the transmittance of the atmosphere. By supplying the IR camera with the required parameters, the FLIR Systems thermographic equipment will use the above general formula to solve for U_{obj} . U_{obj} is the calculated camera output voltage for a blackbody of temperature T_{obj} - a voltage that can be directly converted into true requested object temperature [5].

Creating a blackbody specimen

An isothermal cavity heated to a uniform temperature generates blackbody radiation, called a *cavity radiator*, the characteristics of which are determined solely by the temperature of the cavity. This cavity radiator becomes a necessary tool when determining material radiation characteristics and for calibrating thermographic instruments such as an IR camera.

The construction of a blackbody source is simple. A common blackbody used in IR measurements is a cavity with a small opening (Figure 4). This cavity-type blackbody will have radiation coming in through the opening and undergoes multiple reflections once inside allowing for the radiation to be reflected by the interior surfaces of the cavity before the radiation can escape [6]. The level of blackness, or emissivity, obtained at the aperture is 99.4 ± 0.2 [7] using

the given dimensions (shown below) by *Castrejon-Garcia, et.al.* and is capable of handling almost all wavelengths.

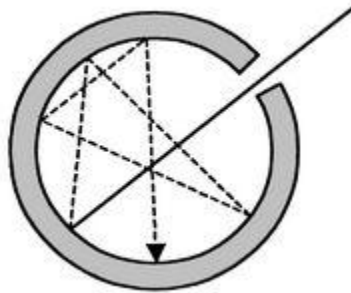


Figure 5 Blackbody cavity

To determine the emissivity of a Ti-6Al-4V specimen, a rectangular prism with outside dimensions of 37 mm x 37 mm x 40 mm (Figure 5) was built via EBM. For the cavity, an orifice diameter of 2.5 mm with a depth of 5 mm was fabricated with an internal spherical cavity of diameter 30 mm (Figure 6). A second sample was also built, a cylinder: 37 mm (diameter) x 40 mm (height), with same dimensions for the internal cavity (Figure 6). It is important to note that the construction of these samples in EBM also helps support the true emissivity value, since emissivity is a function of surface morphology, and therefore the uniqueness of this surface will be the same as future builds in EBM. Once fabricated, the parts were then cleaned to remove unmelted powder from inside the cavity. One specimen was then placed back in the A2 system, the vacuum chamber was activated, and the block was heated to 760°C with the electron beam. The beam is stopped and sequences of images were captured. Using *ThermaCAM Researcher Professional* software, the emissivity of the aperture, which closely resembles a blackbody, was set to 0.99 [7]. Using a spot measurement tool, the temperature of the aperture is recorded. Now the measurement function is moved to the specimen surface. Using the software to determine the emissivity of the sample's surface, or simply equating Stefan-Boltzmann for both surfaces (the aperture and the Ti-6Al-4V surface) and solving for the unknown emissivity, yields the new emissivity value.

Figure 8 is a plot of the emissivity values measured for three samples. Two of the samples used in the experiment were rectangular, and the third was circular (Figure 6) (the geometry had little influence on the emissivity measured). The IR camera has three distinct temperature measurement ranges (-20 °C to 150 °C, 0 °C to 650 °C, and 300 °C to 2000 °C) with their respective calibrations already set in place by the manufacturer; the object measurement range used in this experiment was: 300 °C to 2000 °C. This temperature range makes it possible to achieve a more accurate reading because of its calibration sensitivity to such high temperatures.

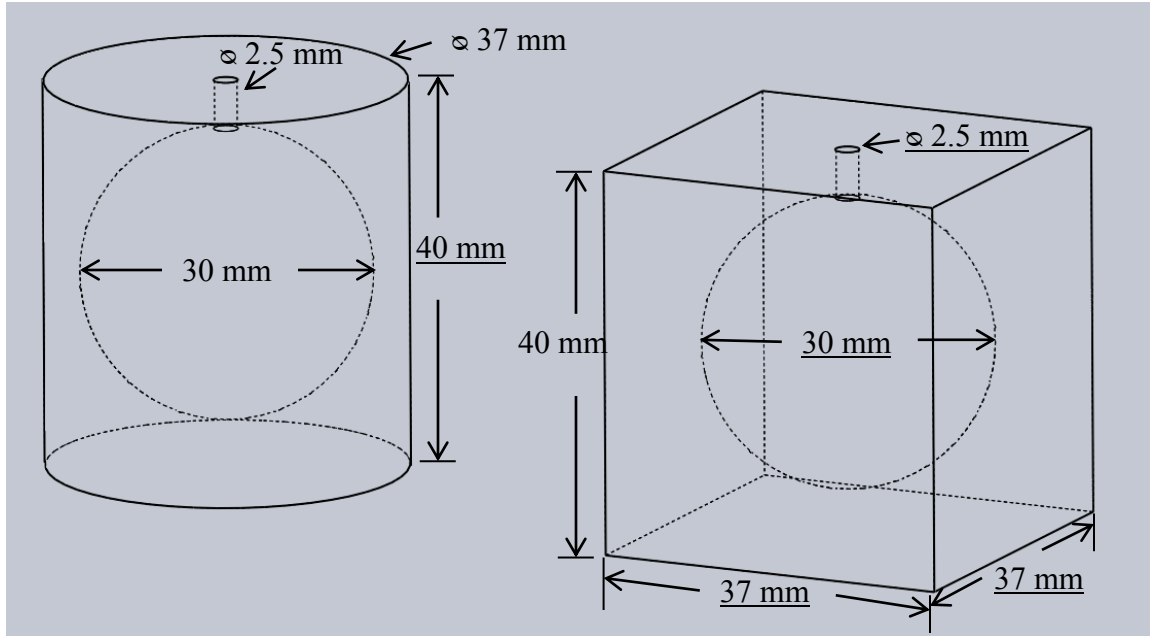


Figure 6 Wire frame view (with hidden lines) of blackbody cavity model specimen-cylinder (left) and rectangular prism (right)

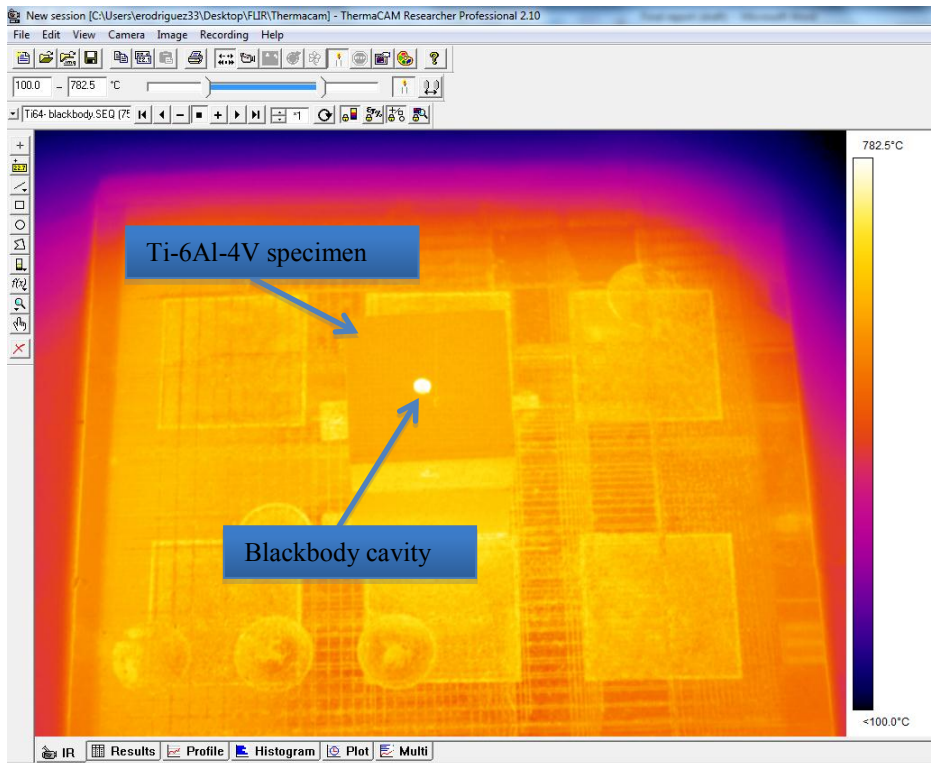


Figure 7 IR image of blackbody cavity (seen here is the orifice)

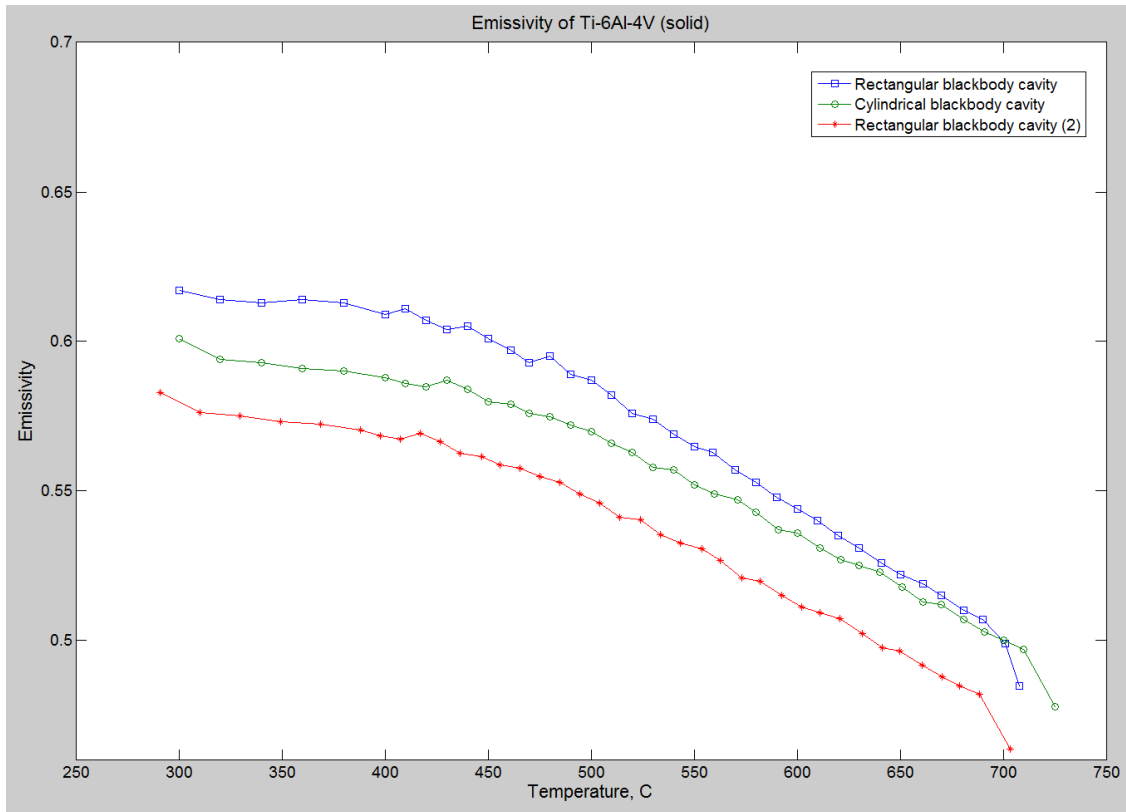


Figure 8 Emissivity plot of Ti-6Al-4V

Measurement Uncertainty Analysis

To test if the temperature reading of the blackbody specimen's aperture was accurate, a thermocouple was inserted inside the cavity (Figure 9) and the specimen was once again heated in the A2 chamber. To determine the total degree of measurement uncertainty associated with the IR camera measurement, the uncertainty of the measurement devices used in the experimental set-up are included. The type K thermocouple used to inside the cavity has a reported uncertainty of $\pm 0.75\%$ of $^{\circ}\text{C}$ reading [8], the thermocouple input module (NI 9213, National Instruments, Austin, TX) has an error of $\pm 1.10^{\circ}\text{C}$ ($\pm 0.03\%$) for the range of 600°C to 800°C [9], the deviation of the IR camera's measurement of the aperture (emissivity set equal to 0.99) to that of the thermocouple inside the cavity was also included in the uncertainty calculation (the major contributor in the percent error). Using the fractional uncertainty equation (or root squares method) [10] given as the uncertainty of the IR camera was determined.

$$\frac{W_T}{T} = \left[\sum \left(\frac{a_i w_{x_i}}{x_i} \right)^2 \right]^{1/2}$$

Where w_{x_i}/x_i is the uncertainty of the instrument, and a_i is the coefficient of the variable used in the respective measurement equation. At the given camera angle, location, and viewing window, the IR camera uncertainty is approximated to be $\pm 5.0\%$ in the temperature range of 465 °C to 760 °C or ± 35 °C at 760 °C - the temperature maintained for Ti-6Al-4V during the build process. It is important to note that there are other possible sources of error that were not included in the calculation, and further work will include identifying these sources, and improving on the experimental set-up to minimize this error calculation.

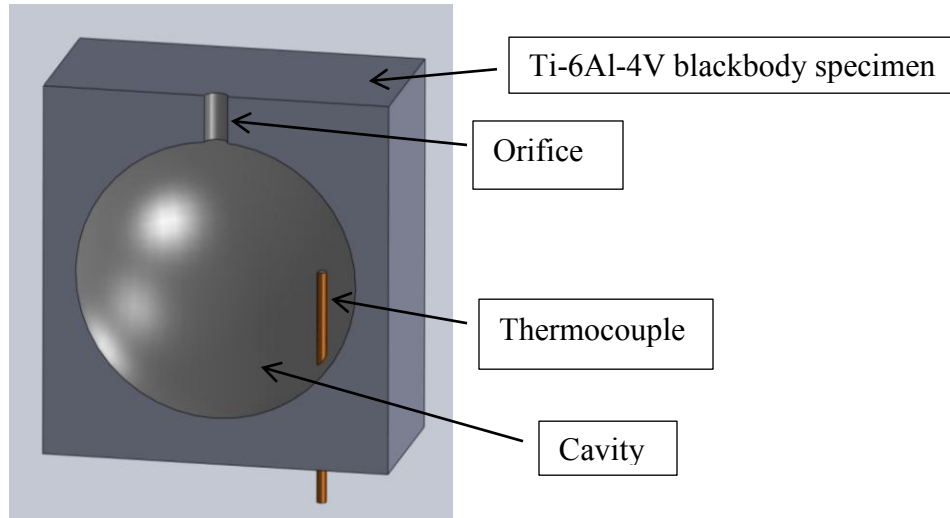


Figure 9 Blackbody cavity radiator with internal thermocouple

Image Analysis

Currently the analysis of images is being carried out manually. The raw images are acquired and uploaded to *ThermaCAM Researcher* where the operator evaluates the images for defects (Figure 10) and non-homogeneous temperature gradients. Figure 10 shows an IR image of cylinders being fabricated of a non-standard material, during the course of build parameter development, it was seen that the build temperature was too high causing the parts to swell, or over-melt.

A part with non-uniform temperature distribution is associated with a defect, sometimes referred to as ‘cold-spots.’ These cold spots will appear in a darker color due to lower-IR emission, a result of a lower temperature or lower local emissivity [3]. Histogram analysis proves an effective method of quantifying these regions of interest (Figure 11). A part with a more consistent temperature will have a higher concentration of pixels within a smaller temperature range, and part with cold-spots will have a higher temperature range of pixel distribution.

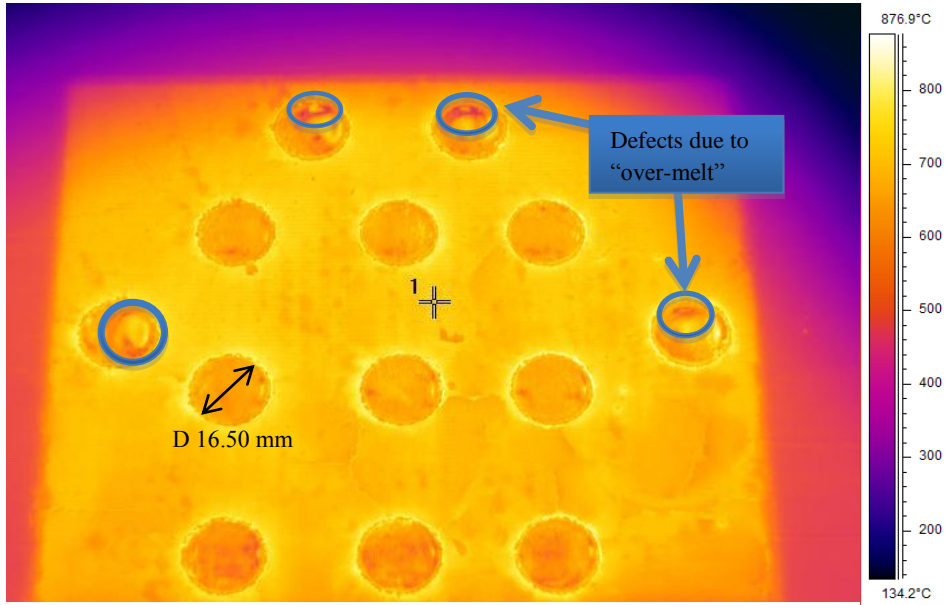


Figure 10 IR image of tensile bars with defects

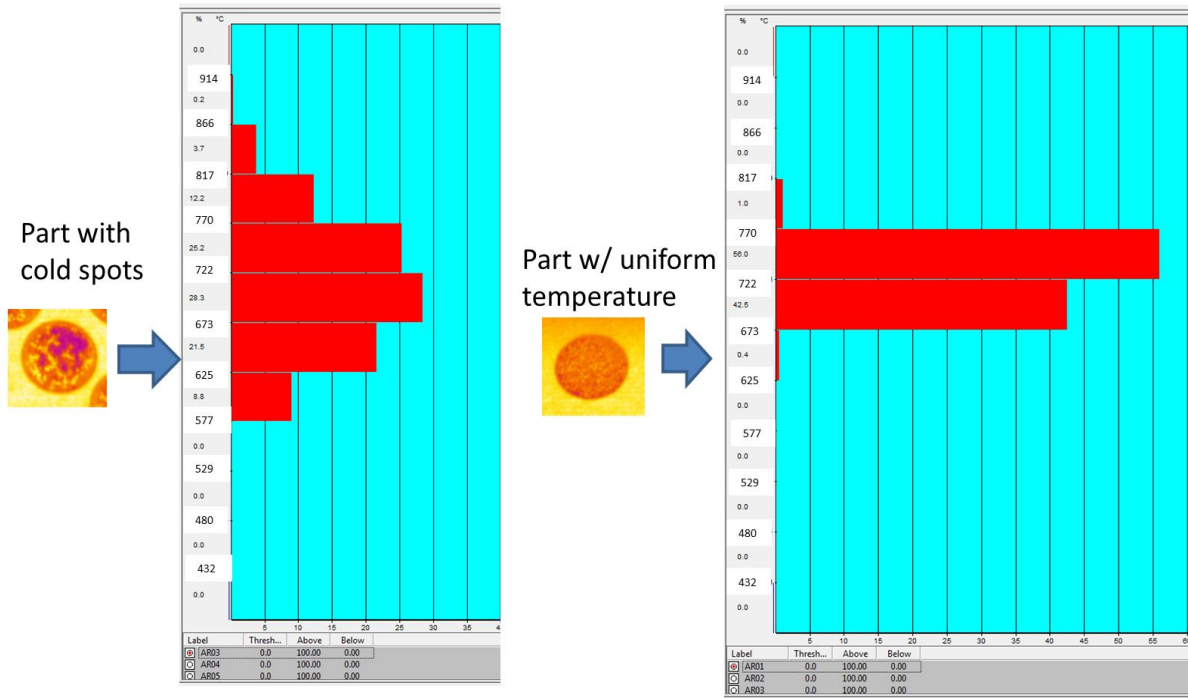


Figure 11 Histogram of an IR image of a circular part with non-uniform temperature (left) compared to part with a uniform temperature (right)

Feedback Control Demonstration

Having the ability to measure surface temperatures during a build enabled this project to modify individual part-parameters for a more consistent build. The experimental setup was designed to analyze how neighboring parts would affect heat transfer to each other in comparison to the heat transfer of a single part (no neighboring parts). The model constructed consisted of a group of nine tensile bars (cylinders) located in one corner, and a single bar in the opposite corner all with equal dimensions, 89 mm tall x 16.50 mm diameter (Figure 12). The parts were manufactured in the build chamber using the same layout seen in the model. That is, the grouped cylinders are towards the front of the chamber and the single cylinder towards the rear.

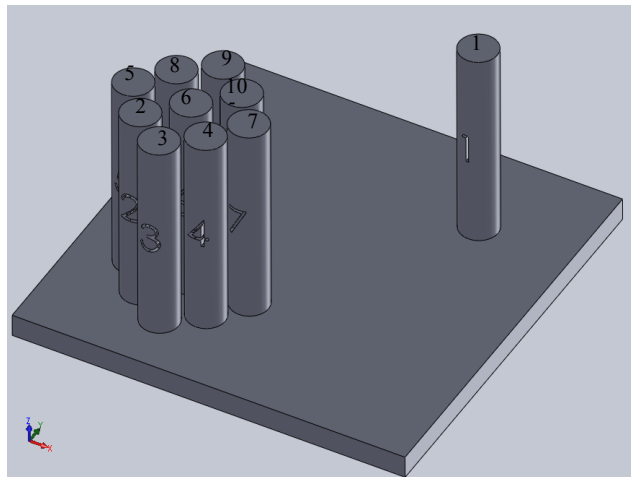


Figure 12 Tensile bar build layout for part location test

An IR image of the build's surface was captured after every melt cycle for the entire course of the build. The results obtained from the images demonstrate that non-uniform temperatures do exist on the build's surface area. By analyzing an IR image of a standard build (i.e., no build parameter modification) at a build height equal to 36.24 mm, one can see a temperature difference of up to 57 °C between cylinders number '5' and number '7' (see the average temperature results column in Figure 13).

The build parameters of individual parts were modified in an attempt to achieve more uniform surface temperatures. The temperature difference among the same cylinders was successfully reduced to 27 °C (Figure 14). The two parameters modified during the build were the speed function, which controls the scanning speed of the beam during melting, and the beam's current. The speed function's initial value was set at 36 and was gradually reduced to 5 in decrements of 4 and 5. The beam current was incrementally increased from 17 mA to 29 mA.

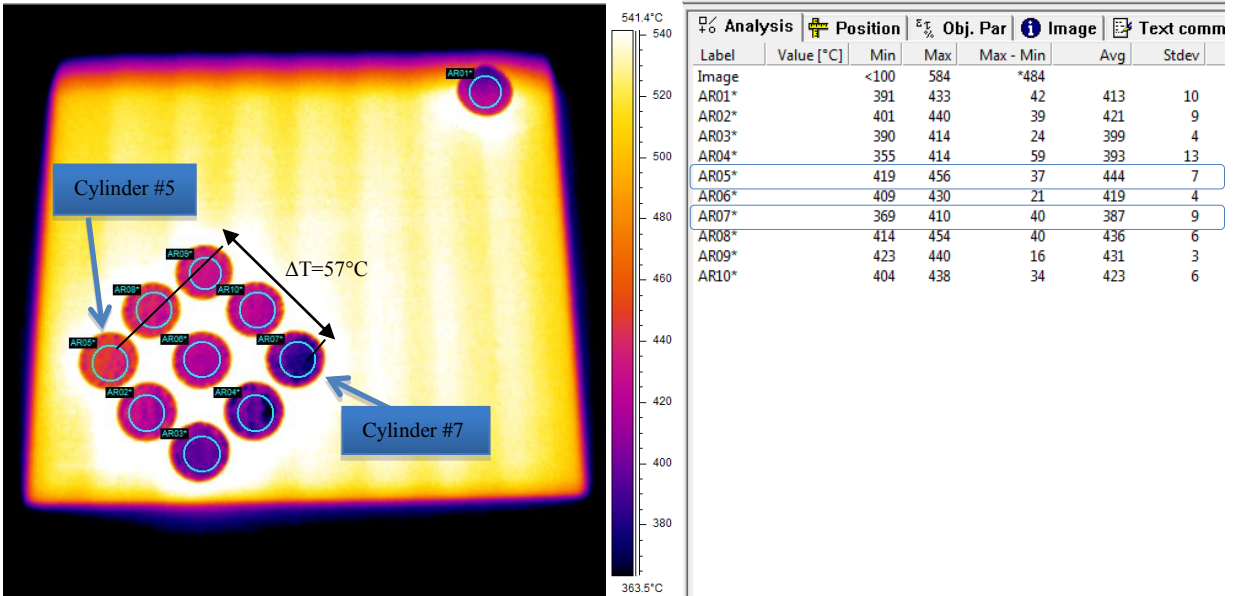


Figure 13 IR image of build surface at z=36.24 mm (1.42”) - no parameter modification

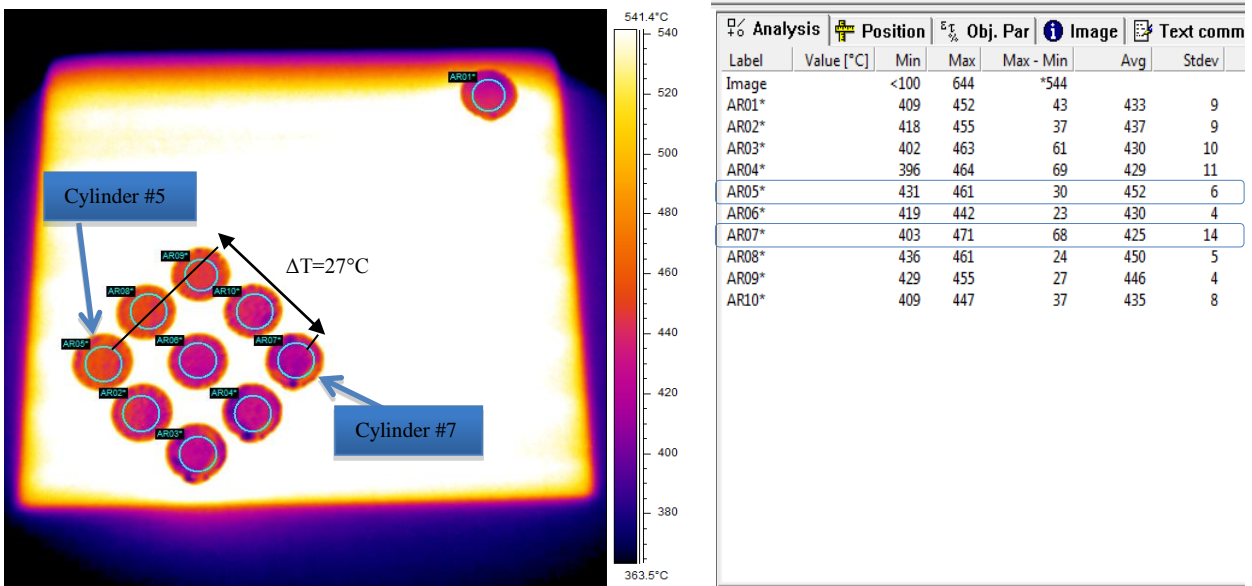


Figure 14 IR image of build surface at z=86.40 mm (3.4”) - with parameter modification

Discussion

It is important to note that the temperature readings gathered during this experiment are not true temperatures, that is, they are only relative. The calibration procedure discussed earlier is designed to acquire a true temperature reading from an already fabricated solid part. During the course of a build, the solid part is surrounded by powder with a much higher emissivity [3],

which contributes to the reflective sources that the camera reads. This emissivity difference is evident in Figures 13 and 14 where the powder surrounding the parts appears to be hotter (brighter color) than the part (darker color), when in fact it is the recently melted part that is hotter. There is also transient temperature decay factors that need to be researched further, as this may significantly affect measurements obtained, since a single image is captured only after all parts have been melted, the parts melted first in the cycle may experience some decay in temperature and may have a lower temperature than those melted last (e.g. cylinder '1' may be melted first, and cylinder '3' last).

Further work is needed to obtain the emissivity of the metal powder – the main contributor to the reflective temperature. Additionally, knowing the emissivity of the powder will allow for the measurement of the heat up rate of the newly deposited powder layer on the part surface to investigate and verify quality of the powder before it goes through the melt cycle. More work is also needed to further test this hypothesis and determine if the temperature differences measured (e.g. $\Delta T=57^{\circ}\text{C}$) affect part quality, microstructure - mechanical testing, SEM, and metallographic analyses can be used for these analyses.

Future Work

Future work with the EBM and IR camera integration will consist of activities which allow both the systematic detection of macro-defects as well as correlation of microstructural anomalies and defects with thermal history data. Also planned is the development of a predictive control system whereby data from each IR image will be used as initial values in numerically solved parabolic differential equations to predict surface temperature evolution between electron beam scans. This will allow intervention of the build process and spatial adjustments in electron beam intensity to ensure compliant temperature profiles are maintained throughout the build process.

The strategy for macro-defect detection involves a digital comparison of thermal images from each layer of the build to target images developed from the build information file. A threshold of acceptance will be determined experimentally and applied to a detection algorithm. The determination of a defect can either take place during part fabrication or after the build is complete. In the first case, a detected defect may result in the interruption of the build process pending input from the system user. The output of this detection system will be a report indicating part acceptance or rejection. Post-build part inspections (destructive and non-destructive) will confirm effectiveness of the detection system. The study of resulting microstructure and correlation to the EBM process will require statistically valid sampling of specimen micrographs mapped to their location within the part and orientation relative to the part build axis. This correlation activity will also include appropriate mechanical testing to complement study of microstructure.

Of utmost significance in the integration of thermal imaging capability with the EBM system is the possibility of developing a real-time predictive control system. The nature of the build process is such that ample time is available between beam cycles to allow numerical processes to be carried out and beneficial changes to be made to process parameters. Together with experimentally determined properties such as emissivity and thermal conductivity of the metal powders (and the consolidated regions), temperature data captured immediately after a scan can be used to simulate the thermal environment as it evolves prior to electron beam scanning on the subsequent layer. Initial efforts in this direction will involve the use of a PC running LabVIEW®, custom simulation and control software, and a Digital Signal Processor (DSP) development kit. Ultimately, a stand-alone system will be developed using a Field Programmable Gate Array (FPGA) and DSP chip along with other needed components

Also, the development of a procedure to determine the metal-powder emissivity, which will help accurately quantify the entire surface temperatures. Additionally, fundamental correlations between process parameters, the melt's temperature, part placement, and the part properties should be established. A thorough investigation of the transient heat transfer dynamics occurring inside the vacuum chamber will also be investigated.

Conclusions

A thermal imaging system was successfully integrated into the *Arcam A2* EBM system. To achieve the objective of acquiring temperature distributions on the surface bed, solutions and procedures were developed such as installing an IR camera within the *Arcam A2* EBM system and determining the emissivity of a metal sample constructed in the EBM process. Determining the emissivity of an EBM fabricated part allows for temperature reading with a certainty of $\pm 5\%$ with the current experimental setup, but more work is needed to account for other influencing factors that may minimize this uncertainty.

An automated solution was developed to acquire IR images during the build. Additionally, influencing factors (e.g. part placement, neighboring parts) on the non-uniformity of the surface temperature were explored. The immediate benefits of the incorporated thermal imaging system include the in-process identification of over-melting, temperature distribution magnitudes, internal part defects, and temperature gradient control— all of which have an effect on part quality. Thermal imaging is a suitable feedback monitoring system for this powder bed process. Thermal imaging will enable measurement of the effects of process parameters (such as speed function and beam's current) on the melt temperature, therefore allowing the implementation of layer-by-layer build modifications to maintain uniform or prescribed temperature distributions within the build chamber, resulting in improved and more controlled part quality.

References

- [1] Cormier, D., Harryson, O., West., H., (2004). *Characterization of H13 steel produced via electron beam melting*. Rapid prototyping journal, vol. 10, 1, pp. 35-41.
- [2] Weger, A., Witt, G., (2011). *Process monitoring in laser sintering using thermal imaging*. German Research Foundation DFG, pp. 405-414.
- [3] Schwerdtfeger, J., Singer, R.F., Körner, C. (2012). *In situ flaw detection by IR-imaging during electron beam melting*. Rapid Prototyping Journal, Vol. 18, 4, pp. 259-263.
- [4] Maldague, X.P.V. (2001). *Theory and practice of infrared technology for nondestructive testing*. New York, NY: John Wiley & Sons, Inc.
- [5] FLIR's User Manual- Thermacam Research Professional 2.10 (2010).
- [6] Cengel, Y.A. (2007). *Heat and mass transfer: A practical approach*. New York, NY: McGraw-Hill.
- [7] Castrejon-Garcia, R., Castrejon-Pita, J.R., Castrejon-Pita, A.A. (2010). *Design, development, and evaluation of a simple blackbody radiative source*. AIP Review of Scientific Instruments.
- [8] Nakos, J.T. (2004). *Uncertainty analysis of thermocouple measurements used in normal and abnormal thermal environments at Sandia's Radiant Heat Facility and Lurance Canyon Burn Site*. Albuquerque, NM: Sandia National Laboratories.
- [9] N.I. (2009). *NI 9213 Operating instructions and specifications*. National Instruments.
- [10] Holman, J.P. (2001). *Experimental methods for engineers*. Boston, MA: McGraw-Hill.
- [11] Klinger, T., (2003). *Image processing with labview and IMAQ vision*. Upper Saddle River, NJ: Prentice Hall.
- [12] Cormier, D., Harryson, O., West., H., (2004). *Characterization of H13 steel produced via electron beam melting*. Rapid Prototyping Journal, Vol. 10, 1, pp. 35-41.
- [13] Elfstrom, I. (2011). *EBM Process*. Power point presentation.